

LOZI MAPS WITH MAX FUNCTION AND ITS APPLICATION

ABDELLAH MENASRI

Received 17 July, 2022; accepted 29 January, 2023; published 28 February, 2023.

HIGHER NATIONAL SCHOOL OF FORESTS, KHENCHELA, ALGERIA.
abdellah.menasri70@gmail.com

ABSTRACT. In this paper, we study the Lozi map by replacing the piecewise linear term in the first equation by the function $\max(f(x, y); g(x, y))$ such that f and g are two arbitrary functions in \mathbb{R}^2 . This is a family model that allows us to study several new piecewise-smooth maps. We demonstrate that these models converge to a robust chaotic attractor and give some applications of these models in the real world.

Key words and phrases: Lozi maps; Max functions; Border collision bifurcations; Robust chaos; Applications.

2010 Mathematics Subject Classification. 37E05, 37G05, 37G10.

1. INTRODUCTION

Some systems, even simple ones, can be deterministic, without being predictable. Even if the future state of the system is completely determined by its present state, it is therefore not necessarily possible to predict the future of the system beyond a very short time. Scientists believed that if you could isolate a system from the influences of its environment and describe it using a small number of variables, it would be both deterministic and predictable. The rather formidable development of the theory of dynamical systems has made it possible to highlight the fairly banal a posteriori observation that, to be predictable, the system must be stable (there must not only be small uncertainties on the initial state of the system occur). Magnify too quickly, otherwise any prediction of the future behavior of the system becomes illusory. So said meteorologist Edward Lorenz in his interpretation of the mathematical model he discovered in 1963.

1.1. Lorenz system. In 1963, meteorologist Edward Lorenz was the first to highlight the probable chaotic character of meteorology. The Lorenz model, also called Lorenz dynamic system or Lorenz oscillator, is a simplified modeling of meteorological phenomena based on fluid mechanics. This model is a three-dimensional dynamic system that generates chaotic behavior under certain conditions. Lorenz's model had important repercussions by showing the possible limits on the ability to predict long-term climatic and meteorological evolution. This is an important part of the theory that the atmospheres of planets and stars can have a wide variety of quasi-periodic regimes and are subject to abrupt and seemingly random changes. It is also a useful example for the theory of dynamical systems serving as a source for new mathematical concepts [3], [5], [7] The Lorenz system is defined by:

$$\begin{cases} \frac{dx}{dt} = \sigma(y - x) \\ \frac{dy}{dt} = \rho x - y - xz \\ \frac{dz}{dt} = xy - \beta z \end{cases}$$

where σ , ρ and β are three strictly positive, fixed parameters. The system coming from the simplification of the equations governing Rayleigh-Bénard convection, the parameters are named after their physical origin: σ is the Prandtl number, and ρ incorrectly called "Rayleigh number", for $\sigma = 10$, $\beta = 8/3$ and $\rho = 28$, the Lorenz system exhibits chaotic behavior which results in a chaotic attractor as shown in Figure 1.

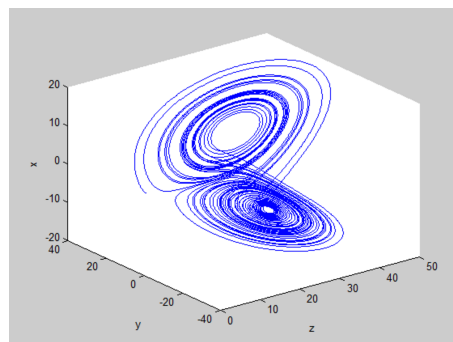


Figure 1: The Lorenz attractor.

1.2. Henon maps. The Henon map [8], [10] was introduced by Michel Henon as a simplification of the Poincare section of the Lorenz attractor. The latter shows how the different variables

of the dynamical system evolve over time in a non-periodic trajectory. Henon’s map is defined by:

$$\begin{cases} x_{n+1} = 1 + y_n - ax_n^2 \\ y_{n+1} = bx_n \end{cases}$$

where a and b are nonzero real parameters. The Henon map presents a chaotic attractor for $(a, b) = (1.4, 0.3)$ call the Henon attractor [1], [4], [6] represented in Figure 2. We note that the Henon dynamical system is not conservative, because the Jacobian of the transformation is constant and equals $-b$, which is different from unity in the interesting cases.

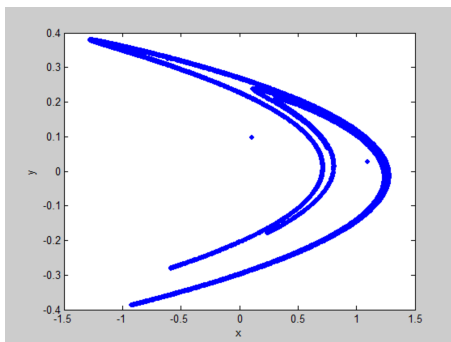


Figure 2: The Henon attractor.

1.3. **Lozi maps.** In 1978, Lozi introduces in a short note a new chaotic map [9], [10] in two dimensions, the equations and attractors resemble those of the famous Henon map, quite simply, a quadratic term in it is replaced by another linear term by pieces in the first equation, this makes it possible to rigorously prove the chaotic character of certain attractors [1], [6] and a detailed analysis of their basins of attraction. The Lozi map is defined by:

$$\begin{cases} x_{n+1} = 1 + y_n - a|x_n| \\ y_{n+1} = bx_n \end{cases}$$

where a and b are nonzero real parameters. Inside the region where the orbits remain bounded, the Lozi map can present both regular and chaotic behaviors depending on the values of the two parameters a and b as illustrated in Figure 3.

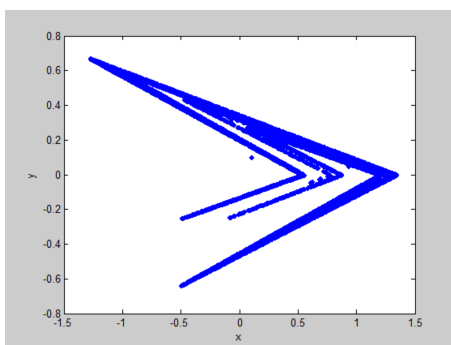


Figure 3: The Lozi attractor.

1.4. Border collision bifurcations. If a fixed point loses its stability while in either side, the bifurcations obtained can be classified under the generic classes of smooth bifurcations [12]. But what if a fixed point crosses the boundary as a parameter is varied? Eigenvalues can change from one value to another value in the unit circle. The resulting bifurcations are called boundary collision bifurcations. So in switching dynamical systems the bifurcation sequence is governed by a complex interaction between smooth bifurcations and boundary collision bifurcations. The different types of smooth bifurcations are well known. What are the different types of boundary collision bifurcations? The answer to this question depends on the nature of the boundary and also the functions on both sides of the boundary. In two-dimensional systems, the classification of fixed points will depend on the continuity of the function across the boundary and the Jacobian elements at both sides of the boundary. There are the following possibilities:

1. The function is continuous, but the Jacobian changes discontinuously across the boundary.
2. Determinant greater than unity on one side of the boundary (fixed point can be repulsive). Birth of a torus by the bifurcation collision of the border.
3. The function as well as the Jacobian are discontinuous across the border.
4. Maps with a square root singularity. For mechanical systems experiencing soft impacts, the determinant has been shown to remain constant, but the Jacobian trace shows a square root singularity.
5. System with a different dimension on both sides of the border.

1.5. The robust chaos. Some chaotic dynamical systems give two types of chaotic attractors. The first is called fragile chaos, attractors disappear with perturbations of a parameter, or coexist with other attractors [2], [5], [13], [16], [17]. The second is called the robust chaos, this type is characterized by the absence of periodic orbits and only accepts coexistence in the neighborhood of the parameter space. The existence of these orbits in certain chaotic regions means that a small change in the parameters destroys the chaos, which implies the fragility of this type of chaos. We say a chaotic attractor is robust if, by its parameter values, there exists a neighborhood in the parameter space without periodic attractor and the chaotic attractor is unique in this neighborhood.

2. LOZI MAPS WITH MAX FUNCTION

In this work, we show that robust chaos [5], [11], [15], [16] can occur in piecewise continuous systems and obtain the conditions for its occurrence. We illustrate this phenomenon on an application of Lozi by replacing the term $|x|$ by function $\max(f(x, y), g(x, y))$, where f and g are two arbitrary functions. This is a general model that allows us to study several new piecewise smooth applications. We have given some conditions that allow these models to converge to robust chaotic attractors [17].

The family of Lozi applications with the max function is defined by:

$$(2.1) \quad M(x, y) = \begin{pmatrix} 1 - a \max(f(x, y), g(x, y)) + by \\ x \end{pmatrix}$$

Where f and g are two arbitrary functions and a, b are the bifurcation parameters. We can write the map M in the form:

$$(2.2) \quad M(x, y) = \begin{cases} M_A(x, y) = \begin{pmatrix} 1 - af(x, y) + by \\ x \end{pmatrix} & \text{if } (x, y) \in R_A \\ M_B(x, y) = \begin{pmatrix} 1 - ag(x, y) + by \\ x \end{pmatrix} & \text{if } (x, y) \in R_B \end{cases}$$

Where

$$(2.3) \quad \begin{cases} R_A = \{(x, y) \in \mathbb{R}^2 : f \geq g\} \\ R_B = \{(x, y) \in \mathbb{R}^2 : f \leq g\} \end{cases}$$

the boundary between them is: $\Pi = \{(x, y) \in \mathbb{R}^2 : f(x, y) = g(x, y)\}$. Suppose both functions f, g and their derivatives are continuous, hence the map M is continuous and its derivative is not continuous on the boundary Π . We assume that the map (2.1) has two fixed points $P_A(x_A, y_A)$ and $P_B(x_B, y_B)$ on the two sub-regions R_A and R_B respectively, the two matrices of the map (2.1) evaluated at the two points P_A, P_B in R_A et R_B respectively are

$$(2.4) \quad J_A = \begin{pmatrix} -a \frac{\delta f}{\delta x}(x_A, y_A) & -a \frac{\delta f}{\delta y}(x_A, y_A) + b \\ 1 & 0 \end{pmatrix}$$

$$(2.5) \quad J_B = \begin{pmatrix} -a \frac{\delta g}{\delta x}(x_B, y_B) & -a \frac{\delta g}{\delta y}(x_B, y_B) + b \\ 1 & 0 \end{pmatrix}$$

Therefore, the determinants of the two matrices given in (2.4), (2.5) are

$$Det_A = a \frac{\delta f}{\delta y}(x_A, y_A) - b, \quad Det_B = a \frac{\delta g}{\delta y}(x_B, y_B) - b$$

respectively. The map M is a dissipative dynamic system when

$$(2.6) \quad \left| a \frac{\delta f}{\delta y}(x_A, y_A) - b \right| < 1, \quad \left| a \frac{\delta g}{\delta y}(x_B, y_B) - b \right| < 1$$

Therefore, we have

$$(2.7) \quad \begin{cases} \frac{-b+1}{a} < \frac{\delta f}{\delta y}(x_A, y_A) < \frac{b+1}{a} \text{ and } \frac{-b+1}{a} < \frac{\delta g}{\delta y}(x_B, y_B) < \frac{b+1}{a} \text{ if } a > 0. \\ \frac{b+1}{a} < \frac{\delta f}{\delta y}(x_A, y_A) < \frac{-b+1}{a} \text{ and } \frac{b+1}{a} < \frac{\delta g}{\delta y}(x_B, y_B) < \frac{-b+1}{a} \text{ if } a < 0. \end{cases}$$

2.1. Analytical results. In this subsection, we have given a rigorous proof of certain conditions on the parameters a and b , so that the map (2.1) converges to a robust chaotic attractor. The nature of the boundary collision bifurcations depends on the local nature of the map in the vicinity of the fixed points, so it suffices to look at the piecewise linear approximation on the sides of the boundary. The normal form of the map M in the neighborhood of one of the fixed points at the boundary [12], [14] is given by the form:

$$(2.8) \quad \begin{pmatrix} x_{n+1} \\ y_{n+1} \end{pmatrix} = \begin{cases} \begin{pmatrix} \tau_A & 1 \\ -\delta_A & 0 \end{pmatrix} \begin{pmatrix} x_n \\ y_n \end{pmatrix} + \mu \begin{pmatrix} 1 \\ 0 \end{pmatrix} & \text{if } x_n \leq 0 \\ \begin{pmatrix} \tau_B & 1 \\ -\delta_B & 0 \end{pmatrix} \begin{pmatrix} x_n \\ y_n \end{pmatrix} + \mu \begin{pmatrix} 1 \\ 0 \end{pmatrix} & \text{if } x_n \geq 0 \end{cases}$$

where μ is the bifurcation parameter and $\tau_A, \tau_B, \delta_A, \delta_B$ are the traces and the determinants for the two matrices J_A et J_B valued at P_A et P_B respectively.

Therefore, we have

$$(2.9) \quad \begin{cases} \tau_A = -a \frac{\delta f}{\delta x}(x_A, y_A) \\ \tau_B = -a \frac{\delta g}{\delta x}(x_B, y_B) \\ \delta_A = a \frac{\delta f}{\delta y}(x_A, y_A) - b \\ \delta_B = a \frac{\delta g}{\delta y}(x_B, y_B) - b \end{cases}$$

The border collision bifurcations of the map M depends only on the values of $\tau_A, \tau_B, \delta_A, \delta_B$, then it suffices to study the border collision bifurcations of the normal form (2.8). We consider

the situation where the map M is dissipative on R_A et R_B . i.e., $|\delta_A| < 1$, $|\delta_B| < 1$. we choose τ_A, τ_B satisfying both conditions:

$$(2.10) \quad -(1 + \delta_A) < \tau_A < (1 + \delta_A),$$

and

$$(2.11) \quad -2\sqrt{\delta_B} < \tau_B < 2\sqrt{\delta_B}$$

The previous conditions ensure that the fixed point P_A is a flip attractor and P_B is a clockwise or counterclockwise spiral. Thus, there are no periodic orbits appear. The fixed points in the subregions R_A, R_B are given by

$$(2.12) \quad P_A\left(\frac{\mu}{1 - \tau_A + \delta_A}, \frac{\mu\delta_A}{1 - \tau_A + \delta_A}\right), P_B\left(\frac{\mu}{1 - \tau_B + \delta_B}, \frac{\mu\delta_B}{1 - \tau_B + \delta_B}\right)$$

These points exist for

$$\frac{\mu}{1 - \tau_A + \delta_A} \leq 0 \text{ and } \frac{\mu}{1 - \tau_B + \delta_B} \geq 0$$

Depending on (2.7),(2.10) and (2.11) we get

$$(2.13) \quad -(1 + a\frac{\delta f}{\delta y}(x_A, y_A) - b) < -a\frac{\delta f}{\delta x}(x_A, y_A) < (1 + a\frac{\delta f}{\delta y}(x_A, y_A) - b),$$

and

$$(2.14) \quad -2\sqrt{a\frac{\delta g}{\delta y}(x_B, y_B) - b} < -a\frac{\delta g}{\delta x}(x_B, y_B) < 2\sqrt{a\frac{\delta g}{\delta y}(x_B, y_B) - b}.$$

Consequently, we have

$$(2.15) \quad -1 + b - a\frac{\delta f}{\delta y}(x_A, y_A) < a\frac{\delta f}{\delta x}(x_A, y_A) < 1 - b + a\frac{\delta f}{\delta y}(x_A, y_A),$$

and

$$(2.16) \quad -2\sqrt{a\frac{\delta g}{\delta y}(x_B, y_B) - b} < a\frac{\delta g}{\delta x}(x_B, y_B) < 2\sqrt{a\frac{\delta g}{\delta y}(x_B, y_B) - b}.$$

From (2.14), we get

$$(2.17) \quad 0 < \left(a\frac{\delta g}{\delta x}(x_B, y_B)\right)^2 < 4\left(a\frac{\delta g}{\delta y}(x_B, y_B) - b\right)$$

because of $|\delta_A| < 1$ and $|\delta_B| < 1$, we have

$$(2.18) \quad b - 1 < a\frac{\delta f}{\delta y}(x_A, y_A) < b + 1 \text{ and } b - 1 < a\frac{\delta g}{\delta y}(x_B, y_B) < b + 1$$

Using (2.15), (2.16) and (2.18), we get

$$(2.19) \quad -2 < a\frac{\delta f}{\delta x}(x_A, y_A) < 2 \text{ and } -2 < a\frac{\delta g}{\delta x}(x_B, y_B) < 2$$

So we get

$$(2.20) \quad \left|a\frac{\delta f}{\delta x}(x_A, y_A)\right| < 2 \text{ and } \left|a\frac{\delta g}{\delta x}(x_B, y_B)\right| < 2$$

Theorem 2.1. : We consider the map M defined by:

$$M(x, y) = \begin{pmatrix} 1 - a \max(f(x, y), g(x, y)) + by \\ x \end{pmatrix}$$

Where f and g are two arbitrary functions, a and b represent two real bifurcation parameters. The application M is written in the normal form:

$$\begin{pmatrix} x_{n+1} \\ y_{n+1} \end{pmatrix} = \begin{cases} \begin{pmatrix} \tau_A & 1 \\ -\delta_A & 0 \end{pmatrix} \begin{pmatrix} x_n \\ y_n \end{pmatrix} + \mu \begin{pmatrix} 1 \\ 0 \end{pmatrix} & \text{if } x_n \leq 0 \\ \begin{pmatrix} \tau_B & 1 \\ -\delta_B & 0 \end{pmatrix} \begin{pmatrix} x_n \\ y_n \end{pmatrix} + \mu \begin{pmatrix} 1 \\ 0 \end{pmatrix} & \text{if } x_n \geq 0 \end{cases}$$

We assume that the map M has two fixed points $P_A(x_A, y_A)$ and $P_B(x_B, y_B)$ located on the two sub-regions $R_A = \{(x, y) \in \mathbb{R}^2 : f \geq g\}$, $R_B = \{(x, y) \in \mathbb{R}^2 : f \leq g\}$ respectively. The map M is dissipative on both subregions R_A, R_B . In addition, we also assume that τ_A, τ_B satisfying to $-(1 + \delta_A) < \tau_A < (1 + \delta_A)$, $-2\sqrt{\delta_B} < \tau_B < 2\sqrt{\delta_B}$ respectively. If we have $|a \frac{\delta f}{\delta x}(x_A, y_A)| < 2$ and $|a \frac{\delta g}{\delta x}(x_B, y_B)| < 2$, there is a pair $(a, b) \in \mathbb{R}^2$ ensures the convergence of the map M towards a robust chaotic attractor.

2.2. Possible forms of functions f and g . In this subsection, we have determined some forms of functions f and g using [15]. Here, we have rigorously determined the region of parameters a and b where the map M converges to a robust chaotic attractor. If the two fixed points P_A and P_B given in (2.12) exist, we can write the map M in the normal form (2.8). Thus, we assume

$$(2.21) \quad \delta_A < \frac{\tau_A^2}{4} \text{ and } \delta_B < \frac{\tau_B^2}{4}$$

Therefore, we get using the two inequalities $\tau_A^2 - 4\delta_A > 0$ and $\tau_B^2 - 4\delta_B > 0$. The eigenvalues $\lambda_{A1} = \frac{\tau_A + \sqrt{\tau_A^2 - 4\delta_A}}{2}$, $\lambda_{A2} = \frac{\tau_A - \sqrt{\tau_A^2 - 4\delta_A}}{2}$ respected at R_A and $\lambda_{B1} = \frac{\tau_B + \sqrt{\tau_B^2 - 4\delta_B}}{2}$, $\lambda_{B2} = \frac{\tau_B - \sqrt{\tau_B^2 - 4\delta_B}}{2}$ respected at R_B .

From (2.9), we have

$$(2.22) \quad \tau_A = -a \frac{\delta f}{\delta x}(x_A, y_A),$$

and

$$(2.23) \quad \tau_B = -a \frac{\delta g}{\delta x}(x_B, y_B)$$

For $a \neq 0$, we have

$$(2.24) \quad \frac{\delta f}{\delta x}(x_A, y_A) = -\frac{\tau_A}{a} \neq 0,$$

and

$$(2.25) \quad \frac{\delta g}{\delta x}(x_B, y_B) = -\frac{\tau_B}{a} \neq 0,$$

therefore

$$(2.26) \quad \begin{cases} f(x, y) = \eta x + u(y) : \eta \neq 0 \\ g(x, y) = \mu x + v(y) : \mu \neq 0 \end{cases},$$

where $\eta = -\frac{\tau_A}{a} \neq 0, \mu = -\frac{\tau_B}{a} \neq 0$, and u, v are arbitrary functions of y .

Let us now apply the conditions given in [17]. The first condition is

$$(2.27) \quad \begin{cases} \tau_A > \delta_A + 1 \text{ and } \tau_B < -(1 + \delta_B) \\ \delta_A < 0 \text{ and } -1 < \delta_B < 0 \end{cases}$$

Therefore

$$(2.28) \quad \delta_A < \min(-\eta a - 1, 0) \text{ and } -1 < \delta_B < \min(\mu a - 1, 0)$$

The second condition is

$$(2.29) \quad \frac{\lambda_{A1} - 1}{\tau_A - 1 - \delta_A} > \frac{\lambda_{B2} - 1}{\tau_B - 1 - \delta_B}$$

Or

$$(2.30) \quad \frac{\lambda_{B2} - 1}{\tau_B - 1 - \delta_A} < \frac{\tau_A - \delta_A - \lambda_{A2}}{(\tau_A - 1 - \delta_A)(\lambda_{A2} - \tau_B)}$$

Therefore

$$(2.31) \quad \frac{\eta a - \sqrt{\eta^2 a^2 - 4\delta_A} + 2}{\eta a + 1 - \delta_A} > \frac{\mu a + \sqrt{\mu^2 a^2 - 4\delta_B} + 2}{\mu a + 1 + \delta_B}$$

Or

$$(2.32) \quad \frac{\mu a + \sqrt{\mu^2 a^2 - 4\delta_B} + 2}{\mu a + 1 + \delta_A} < \frac{\eta a + 2\delta_A - \sqrt{\eta^2 a^2 - 4\delta_A}}{(\eta a + 1 + \delta_A) \left(\mu a - \frac{\eta a + \sqrt{\eta^2 a^2 - 4\delta_A}}{2} \right)}$$

And the third condition is

$$(2.33) \quad (\lambda_{A2} - \tau_B)\lambda_{A1} - \tau_A + \tau_B + \delta_A > 0$$

Therefore

$$(2.34) \quad \mu a \left(\frac{-\eta a + \sqrt{\eta^2 a^2 - 4\delta_A}}{2} \right) + (\eta - \mu)a + 2\delta_A > 0$$

And, on the other hand, we have

$$(2.35) \quad \delta_A = a \frac{\delta f}{\delta y}(x_A, y_A) - b$$

$$(2.36) \quad \delta_B = a \frac{\delta g}{\delta y}(x_B, y_B) - b$$

For $a \neq 0$, we have

$$(2.37) \quad \frac{\delta f}{\delta y}(x_A, y_A) = \frac{\delta_A + b}{a} \neq 0,$$

and

$$(2.38) \quad \frac{\delta g}{\delta y}(x_B, y_B) = \frac{\delta_B + b}{a} \neq 0$$

Therefore

$$(2.39) \quad \begin{cases} f(x, y) = \alpha y + \omega(x) : \alpha \neq 0 \\ g(x, y) = \beta y + \varphi(x) : \beta \neq 0 \end{cases}$$

Where $\alpha = \frac{\delta_A + b}{a} \neq 0$, $\beta = \frac{\delta_B + b}{a} \neq 0$ and ω, φ are arbitrary functions of x . By applying the same conditions above, we obtain the first condition as follows:

$$(2.40) \quad \tau_A > \alpha a - b + 1 \text{ et } \tau_B < -1 - \beta a + b \text{ with } \max(\alpha a, \beta a) < b < \beta a + 1$$

The second condition is

$$(2.41) \quad \frac{\tau_B + \sqrt{\tau_A^2 - 4\alpha a + 4b} - 2}{\tau_A - 1 - \alpha a + b} > \frac{\tau_B - \sqrt{\tau_B^2 - 4\beta a + 4b} - 2}{\tau_B - 1 - \beta a + b}$$

Where

$$(2.42) \quad \frac{\tau_B - \sqrt{\tau_B^2 - 4\beta a + 4b} - 2}{\tau_B - 1 - \alpha a + b} < \frac{\tau_A - 2\alpha a + 2b + \sqrt{\tau_A^2 - 4\alpha a + 4b}}{(\tau_A - 1 - \alpha a + b) \left(\frac{\tau_A - \sqrt{\tau_A^2 - 4\alpha a + 4b}}{2} - \tau_B \right)}$$

and the third condition is

$$(2.43) \quad \tau_B \left(1 - \frac{\tau_A + \sqrt{\tau_A^2 - 4\alpha a + 4b}}{2} \right) - \tau_A + 2\alpha a - 2b > 0$$

Lemma 2.2. *It is numerically proven that for*

$$(2.44) \quad \begin{cases} f(x, y) = -px + qy^2 \text{ and } g(x, y) = px - qy^3 \\ \text{with } 0.7 \leq a \leq 0.9, 0.2 \leq b \leq 0.7, 0.91 \leq p \leq 1 \text{ and } 0.9 \leq q < 1 \end{cases}$$

And

$$(2.45) \quad \begin{cases} f(x, y) = -py + qx^2 \text{ and } g(x, y) = py - qx^3 \\ \text{with } 0.7 \leq a \leq 0.9, 0.2 \leq b \leq 0.3, 0.9 \leq p < 1 \text{ and } 0.9 \leq q \leq 1. \end{cases}$$

1. *The Theorem (2.1) is satisfied for (2.44) and (2.45)*
2. *The model (2.1) can give an infinity of robust chaotic attractors, either for (2.44) or for (2.45)*
3. *The conditions (2.28),(2.31) and (2.34) or (2.28),(2.32) and (2.34) are satisfied for (2.44) and conditions (2.40),(2.41) and (2.43) or (2.40),(2.42) and (2.43) are satisfied for (2.45)*

2.3. Numerical simulation and observation of robust chaotic attractors. In this section, we have numerically studied some examples to demonstrate the effectiveness of the results obtained.

Example 2.1. *In this example, the numerical simulation shows that, for $a = 0.85, b = 0.5, p = 0.99, q = 0.95$ and the initial condition $(1, 1)$, the map (2.44) has a robust chaotic attractor as illustrated in figures 4,5 and 6 . Lyapunov exponents exist with the values $E_1 = -0.755957492608380$ and $E_2 = 0.732395492608378$. It proves that, the map (2.45) has a high sensitivity to the initial condition. Furthermore, the numerical simulation also indicated that this attractor is bounded due to $\max(x_n) = \max(y_n) < 1.75$ and $\min(x_n) = \min(y_n) < 0.26$. moreover the bifurcation diagram illustrated in Figure 7, shows that the map passes through several states, stability, bifurcation and chaos.*

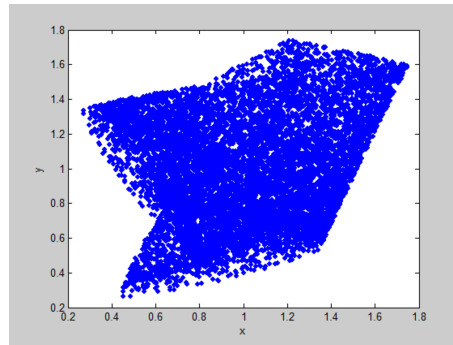


Figure 4: The robust chaotic attractor of map M for $f(x, y) = -px + qy^3$, $g(x, y) = px - qy^3$ with $(a, b) = (0.85, 0.50)$, $(p, q) = (0.99; 0.95)$.

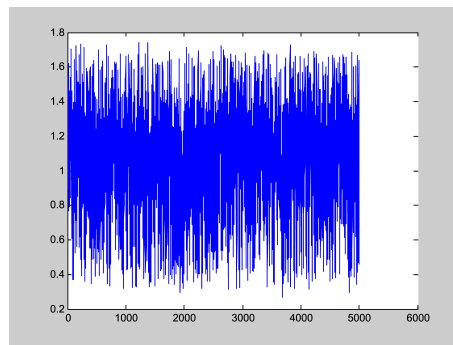


Figure 5: Time series x_n corresponding to the initial condition $(1, 1)$.

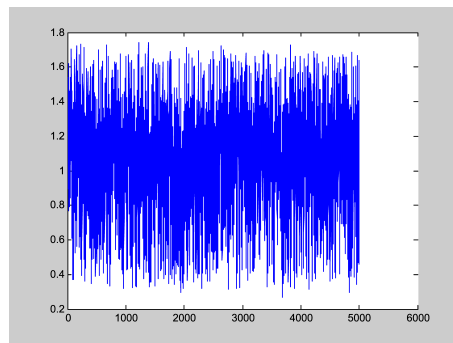


Figure 6: Time series y_n corresponding to the initial condition $(1, 1)$.

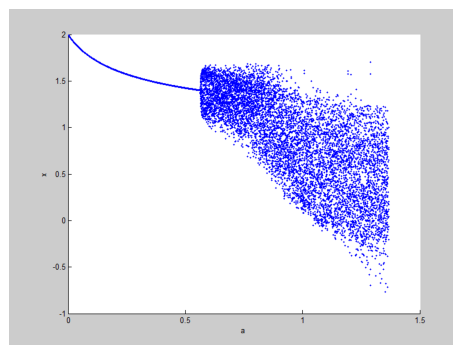


Figure 7: The bifurcation diagram of Lozi maps with max function for: $0 \leq a < 1.5$.

Example 2.2. For $a = 0.75, b = 0.25, p = 0.95, q = 0.99$ and the initial condition $(1, 1)$, the map (2.45) has a robust chaotic attractor completely different from the previous one, as illustrated in figures 8, 9 and 10. Lyapunov exponents exist with the values $E_1 = -0.642765954762084$ and $E_2 = 0.347161540062413$. This proves that the map (2.45) has a high sensitivity to the initial condition. Furthermore, the numerical simulation also indicated that the attractor is bounded since $\max(x_n) = \max(y_n) < 1.32$ and $\min(x_n) = \min(y_n) < 0.68$. moreover the bifurcation diagram illustrated in Figure 11, shows that the map passes through several states, stability, bifurcation and chaos.

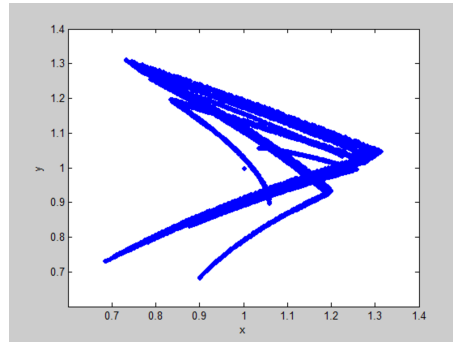


Figure 8: The robust chaotic attractor of the map M for $f(x, y) = -py + qx^3$, $g(x, y) = py - qx^3$ with $(a, b) = (0.75, 0.25)$, $(p, q) = (0.95; 0.99)$.

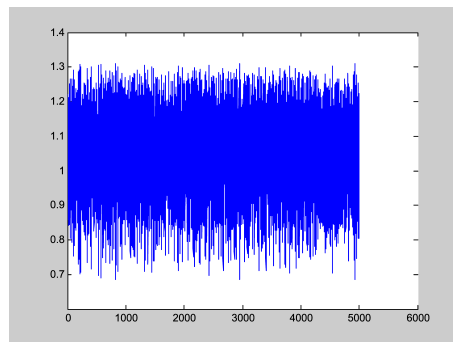


Figure 9: The time series x_n corresponding to the initial condition $(1, 1)$.

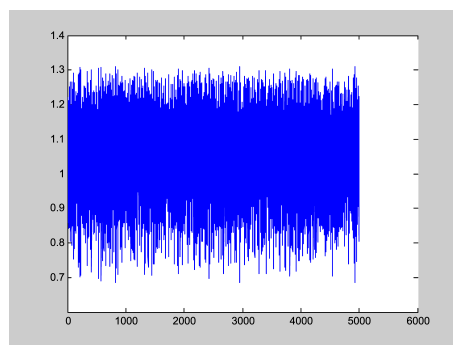


Figure 10: The time series y_n corresponding to the initial condition $(1, 1)$.

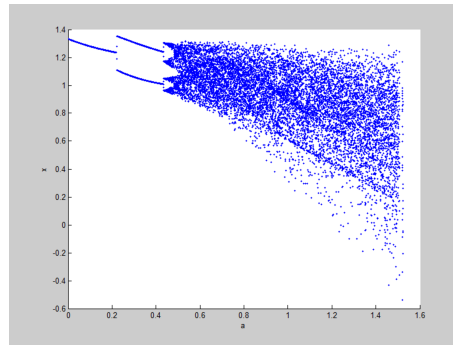


Figure 11: The bifurcation diagram of Lozi maps with max function for: $0 \leq a < 1.6$.

2.4. Some real-world domains where we can apply the Lozi maps with max function. Encryption is a cryptographic process by which we want to make it impossible for anyone who does not have the decryption key to understand a document. This principle is generally linked to the principle of conditional access. Although encryption can make the meaning of a document secret, other cryptographic techniques are needed to communicate securely. To verify the integrity or authenticity of a document, a Message Authentication Code (MAC) or a digital signature are used respectively. It is also possible to take into consideration the analysis of the traffic to which the communication may be subject, since the patterns arising from the presence of communications may be the subject of pattern recognition. To conceal the presence of communications, steganography is used. The security of an encryption system must be based on the secrecy of the encryption key and not on that of the algorithm. The principle of Kerckhoffs assumes that the enemy (or the person who wants to decipher the coded message) knows the algorithm used. Communications security is based on the complex dynamic behaviors provided by chaotic systems. Chaos is a deterministic phenomenon. It is possible to decode the data using this determinism. Chaos communications can be implemented using these properties of chaos. Since the Lozi maps with max function has a distinctive property such that the two functions can be changed every second for example, which means that the cipher can be changed every second. The maps is chaotic for exact values of parameters a and b , but always remains chaotic at each change of the given values of parameters p and q in the two families of Lozi maps with the function max found. We are faced with an infinity of chaotic maps that are difficult to decipher, we can even say that it is impossible to decipher it.

3. CONCLUSION

In this paper, we presented two new families of Lozi maps with max function, we demonstrated that these families converge to a robust chaotic attractor for exact values of parameters a and b , and for infinite values of parameters p and q , we also proved that these families maps can be used in encryption due to these distinctive properties.

REFERENCES

- [1] A. ALAOU, C. ROBERT and C. GREBOGI, Dynamics of a HENON-LOZI-type map, *J. Chaos, Solitons and Fractals*, **12** (2001), pp. 2323–2341.
- [2] A. PRIEL and I. KANTER, Robust chaos generation by a perceptron, *Europhys. Lett.*, **51** (2000), No. 2, pp. 230–236.
- [3] D. J. ALBERS, J. C. SPROTT and W. D. DECHERT, Routes to chaos in neural networks with random weights, *J. Bifurcation and Chaos*, **8** (1998), pp. 1463–1478.

- [4] F. R. MAOROTTO, Chaotic behavior in the HENON mapping, *Journal Com Math. Phys.*, **68** (1979), pp. 187–194.
- [5] G. NAGAMANI, S. RAMASAMY and P. BALASUBRAMANIAM, Robust dissipativity and passivity analysis for discrete-time stochastic neural networks with time-varying delay, *Wiley Online Library*, **21** (2014), pp. 1-12.
- [6] H. SOMPOLINSKY, A. CRISTANTI and H. J. SOMMERS, Chaos in random neural networks, *Phys. Rev. Lett.*, **61** (1998), pp. 259–26.
- [7] M. ANDRECUT and M. K. ALI, On the occurrence of robust chaos in a smooth system, *Modern Physics Letters B*, **15** (2001), pp. 391–395.
- [8] M. BENEDICKS and L. CARLESON, the dynamics of the HENON maps, *Annals of Mathematics*, **133** (1991), pp. 1–25.
- [9] M. MISIUREWICZ, Strange attractor for the LOZI-mapping in Nonlinear dynamics, *Annals of the New York Academy of Sciences*, **357** (1980), pp. 348–358.
- [10] R. LOZI, Un attracteur etrange du type attracteur de HENON, *J. Phys. Colloque C5*, **39** (1978), pp. 9–10.
- [11] R. SENKERIK, MICHAL PLUHACEK and others, Evolutionary control of chaotic LOZI map by means of chaos driven differential evolution, *Springer-Verlag Berlin Heidelberg*, **282** (2014), pp. 371–380.
- [12] S. BANERJEE and C. GREBOJI, Border collision bifurcations in two-dimensional piece-wise smooth maps, *Interdisciplinary Journal of Nonlinear Science*, **21** (1999), pp. 4052–4061.
- [13] S. BANERJEE, J. A. YORK and C. GREBOGI, Robust chaos, *Phys. Rev. Lett.*, **80** (1998), pp. 3049–3052.
- [14] T. GILBERT and J. R. DORFMAN, On the parametric dependeces of a class of non-linear singular maps, *AIM sciences*, **4** (2004), pp. 1–17.
- [15] Z. ELHADJ and J. C. SPOTT, A new simple 2-D piecewise linear map, *The Editorial Office of Jssc & Springer-Verlag Berlin Heidelberg*, **23** (2010), pp. 379–389.
- [16] Z. ELHADJ and J. C. SPOTT, On the robustnessof Chaos in dynamical systems, *Higher Education Press and Springer-Verlag*, **3** (2008), pp. 195–204.
- [17] Z. ELHADJ, A unified piecewise smooth chaotic mapping that contains the HENON and the LOZI systems, *Annual review of chaos theory bifurcations and dynamical systems*, **1** (2012), pp. 50–60.